Critical inclination for absolute/convective instability transition in inverted falling films

Benoit Scheid, Nicolas Kofman, and Wilko Rohlfs

Citation: Physics of Fluids **28**, 044107 (2016); doi: 10.1063/1.4946827
View online: http://dx.doi.org/10.1063/1.4946827
View Table of Contents: http://scitation.aip.org/content/aip/journal/pof2/28/4?ver=pdfcov
Published by the AIP Publishing

Critical inclination for absolute/convective instability transition in inverted falling films

Benoit Scheid,[1,a)] Nicolas Kofman,[2,b)] and Wilko Rohlfs[3,4,c)]
[1]*TIPs, Université Libre de Bruxelles, C.P. 165/67, Avenue F. D. Roosevelt 50, 1050 Bruxelles, Belgium*
[2]*Laboratory of Fluid Mechanics and Instabilities, EPFL, Station 9, 1015 Lausanne, Switzerland*
[3]*Institute of Heat and Mass Transfer, RWTH Aachen University, Augustinerbach 6, 52056 Aachen, Germany*
[4]*Department of Mechanical Engineering, Massachusetts Institute of Technology, 77 Massachusetts Avenue, Cambridge, Massachusetts 02139, USA*

(Received 27 August 2015; accepted 22 March 2016; published online 25 April 2016)

Liquid films flowing down the underside of inclined plates are subject to the interaction between the hydrodynamic and the Rayleigh-Taylor (R-T) instabilities causing a patterned and wavy topology at the free surface. The R-T instability results from the denser liquid film being located above a less dense ambient gas, and deforming into an array of droplets, which eventually drip if no saturation mechanism arises. Such saturation mechanism can actually be provided by a fluid motion along the inclined plate. Using a weighted integral boundary layer model, this study examines the critical inclination angle, measured from the vertical, that separates regimes of absolute and convective instability. If the instability is of absolute type, growing perturbations stay localized in space potentially leading to dripping. If the instability is of convective type, growing perturbations move downwards the inclined plate, forming waves and eventually, but not necessarily, droplets. Remarkably, there is a minimum value of the critical angle below which a regime of absolute instability cannot exist. This minimum angle decreases with viscosity: it is about 85° for water, about 70° for silicon oil 20 times more viscous than water, and reaches a limiting value for liquid with a viscosity larger than about 1000 times the one of water. It results that for any fluid, absolute dripping can only exist for inclination angle (taken from the vertical) larger than 57.4°. *Published by AIP Publishing.* [http://dx.doi.org/10.1063/1.4946827]

I. INTRODUCTION

Falling liquid films on vertical plates or on the upper side of inclined plates are present in many technical applications involving heat and mass transfer, and as such they are well studied.[1–3] Owing to an inherent unstable flow above a critical inclination angle, falling films are characterized by a wavy and distorted topology exhibiting different types of vortices in the trough[4] and the crest[5] of the wave. These instabilities are always of convective type,[3] such that surface perturbations grow in space (in flow direction) and not locally in time, which is confirmed by experiments.[6] For the inverted case of a film flowing down the bottom side of an inclined plate, the flow should also be of convective type if the inclination angle is close to the vertical. However, in the limiting case of a horizontal plate, the Rayleigh-Taylor[7] (R-T) instability deforms the surface. The entire system is described by a balance between destabilizing gravitational forces and stabilizing surface tension forces. The flow is thus of absolute type if the inclination angle is sufficiently close to

a)Electronic mail: bscheid@ulb.ac.be
b)Electronic mail: nicolas.kofman@epfl.ch
c)Electronic mail: rohlfs@wsa.rwth-aachen.de

the horizontal, meaning that perturbations grow locally and are not convected by the flow.[8] As a consequence, there should exist a critical (fluid and flow rate specific) angle at which the instability changes from absolute to convective type. This is what has recently been demonstrated by Brun *et al*.[9] in the limit of negligible inertia and viscous extensional stress strictly valid for low Reynolds number flows. Extending their study to large Reynolds number flows is the aim of this work, which will show non-monotonic absolute/convective transition contrarily to the previous results.

It is well known that the R-T instability in a static and horizontal setup does not exhibit a saturation mechanism,[10] such that either droplet detachment or film rupture occurs within a finite time period.[11] Saturation of the R-T instability and consequently a suppression of dripping can be achieved in different ways, such as applying oscillations in vertical[12] or horizontal[13] direction, an electric field, temperature gradients,[14–16] Marangoni effects,[17] and curvature.[18] In close relation to falling films, Babchin *et al*.[19] have demonstrated that a convective flow in horizontal direction (due to a moving plate at a constant velocity) can result in saturation. This saturation is a result of a non-linear flow-induced and surface-tension-assisted mechanism.

The formation of the three-dimensional R-T instability in an inverted film flow was studied by Lin *et al*.[20] using a model based on the lubrication approximation with neglected effects of inertia. Contrarily to the film flow considered in this study, Lin *et al*. have a non-wetted plate as an initial condition. Although the main focus of their study is on the development of finger-like patterns, they also consider a film destabilized by a Rayleigh-Taylor type instability. They identify for low values of the dimensionless inclination number a propagation front which breaks up into fingers. A further characteristic of the flow is large droplet-like structures which move downwards the plate with a wave speed much faster than the propagation speed of the fingers.

On conditions that the intensity of the saturation mechanism is not sufficiently strong, and, e.g., in the case of an imposed flow rate, the boundary between the convective and absolute instabilities will separate the regime of immediate dripping (see Fig. 1(c)), occurring already in the vicinity of the inlet, from the regime where dripping eventually, but not necessarily, occurs after a sufficiently long inlet length (see Fig. 1(b)). In a similar way the absolute/convective (A/C) boundary separates the regimes of droplet formation in a viscous liquid jet,[21,22] e.g., droplet formation at the nozzle exit or downstream jet breakup, both owing to Plateau-Rayleigh instability.

In Section II, a set of low-dimensionality models based on the weighted integral boundary layer approach will be proposed and hierarchized in terms of their degree of approximation. In Section III, we will present the methodology to identify the A/C transition of a falling liquid film on the underside of an inclined plate subject to R-T instability. A special characteristic of this flow configuration is that both the R-T instability and the convective liquid transport along the inclined

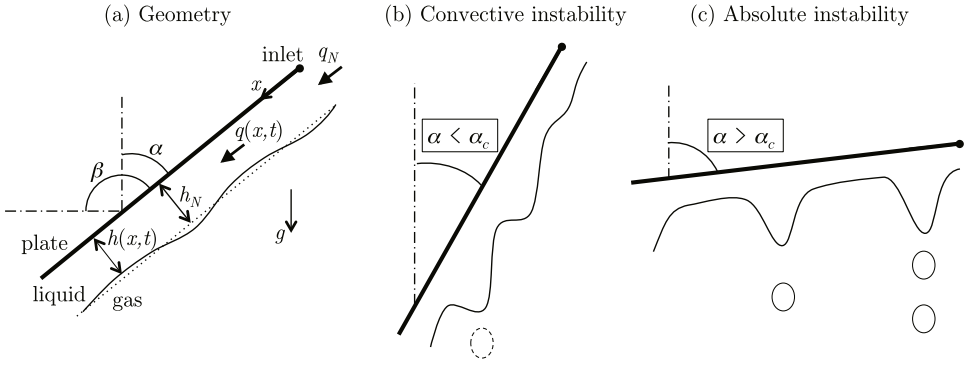

FIG. 1. Sketch of an inverted falling film, a situation that is always unstable: (a) any perturbation around the unperturbed flat film solution will grow in time and either be convected with the flow (b) or be localized in space (c), in the case of which dripping already occurs in the vicinity of the inlet in absence of nonlinear saturation. Note that dripping can eventually, but not necessarily, occur in convective instability as represented by the dashed droplet. The critical angle α_c separates the two regimes of instability.

plate are driven by gravity. Thus, the cotangent of the inclination angle taken from the horizontal determines the ratio between the two coupled mechanisms. In Section IV, and after having shown the differences and specificities of the various models, the influence of two different conservation conditions, e.g., imposed film thickness and imposed flow rate on the A/C transition, is examined. Further, a minimum critical inclination angle for convective instability in falling films is presented. In Section V, we discuss the relevancy of the A/C transition in light of time-dependent simulations of wavepackets, whereas conclusions are given in Section VI.

II. MODELING

The geometry of an inverted falling film under the field of gravity g is sketched in Fig. 1(a) where β is the inclination angle from the horizontal and $\alpha = \beta - \pi/2$ is the inclination angle taken from the vertical, the two angles being used in the paper. The unperturbed flat film thickness is denoted h_N, and q_N is the specific volumetric flow rate (flow rate per unit width) at the inlet. For the evolution of the film flow, the *full second-order model* obtained by Ruyer-Quil and Manneville[23] is considered, whose derivation is briefly detailed in Appendix A. This model consists in four coupled evolution equations for the local film thickness $h(x,t)$, the local flow rate $q(x,t)$, and two corrections of the flow rate $s_1(x,t)$ and $s_2(x,t)$ accounting for the departure from the parabolic velocity profile due to second-order inertia effects. The ordering refers to the classical gradient expansion,[3] such as second-order terms contain second-order derivatives in space (x). Using h_N as the scale for the thickness, and $3q_N$ as the scale for the flow rate, the dimensionless equations are

$$\partial_t h = -\partial_x q, \tag{1a}$$

$$\begin{aligned}\delta\partial_t q = {} & \frac{5}{6}h - \frac{5}{2}\frac{q}{h^2} - \frac{5}{6}\zeta h\,\partial_x h + \frac{5}{6}h\partial_{xxx}h + \delta\partial_t s_1 + \delta\partial_t s_2 \\ & + \delta\left[-4\frac{q s_1\partial_x h}{h^2} - \frac{18}{7}\frac{q s_2\partial_x h}{h^2} + \frac{13}{3}\frac{s_1\partial_x q}{h} + \frac{17}{7}\frac{s_2\partial_x q}{h}\right. \\ & \left. + 3\frac{q\partial_x s_1}{h} + \frac{27}{14}\frac{q\partial_x s_2}{h} + \frac{9}{7}\frac{q^2\partial_x h}{h^2} - \frac{17}{7}\frac{q\partial_x q}{h}\right] \\ & + \eta\left[4\frac{q}{h^2}(\partial_x h)^2 - \frac{9}{2h}\partial_x q\partial_x h - 6\frac{q}{h}\partial_{xx}h + \frac{9}{2}\partial_{xx}q\right],\end{aligned} \tag{1b}$$

$$\begin{aligned}\delta\partial_t s_1 = {} & \frac{1}{10}h - \frac{3}{10}\frac{q}{h^2} - \frac{126}{5}\frac{s_1}{h^2} - \frac{126}{5}\frac{s_2}{h^2} - \frac{1}{10}\zeta h\partial_x h + \frac{1}{10}h\partial_{xxx}h \\ & + \delta\left[-\frac{3}{35}\frac{q^2\partial_x h}{h^2} + \frac{1}{35}\frac{q\partial_x q}{h} + \frac{108}{55}\frac{q s_1\partial_x h}{h^2} - \frac{5022}{5005}\frac{q s_2\partial_x h}{h^2}\right. \\ & \left. - \frac{103}{55}\frac{s_1\partial_x q}{h} + \frac{9657}{5005}\frac{s_2\partial_x q}{h} - \frac{39}{55}\frac{q\partial_x s_1}{h} + \frac{10\,557}{10\,010}\frac{q\partial_x s_2}{h}\right] \\ & + \eta\left[\frac{93}{40}\frac{q(\partial_x h)^2}{h^2} - \frac{69}{40}\frac{\partial_x h\partial_x q}{h} + \frac{21}{80}\frac{q\partial_{xx}h}{h} - \frac{9}{40}\partial_{xx}q\right],\end{aligned} \tag{1c}$$

$$\begin{aligned}\delta\partial_t s_2 = {} & \frac{13}{420}h - \frac{13}{140}\frac{q}{h^2} - \frac{39}{5}\frac{s_1}{h^2} - \frac{11\,817}{140}\frac{s_2}{h^2} - \frac{13}{420}\zeta h\partial_x h + \frac{13}{420}h\partial_{xxx}h \\ & + \delta\left[-\frac{4}{11}\frac{q s_1\partial_x h}{h^2} + \frac{18}{11}\frac{q s_2\partial_x h}{h^2} - \frac{2}{33}\frac{s_1\partial_x q}{h} - \frac{19}{11}\frac{s_2\partial_x q}{h} + \frac{6}{55}\frac{q\partial_x s_1}{h} - \frac{288}{385}\frac{q\partial_x s_2}{h}\right] \\ & + \eta\left[-\frac{3211}{4480}\frac{q(\partial_x h)^2}{h^2} + \frac{2613}{4480}\frac{\partial_x h\partial_x q}{h} - \frac{2847}{8960}\frac{q\partial_{xx}h}{h} + \frac{559}{2240}\partial_{xx}q\right],\end{aligned} \tag{1d}$$

where δ is the reduced Reynolds number, ζ is the reduced inclination number, and η is the viscous extensional number, whose definitions are given in Sec. III (see Eq. (9)). The parameter $\delta > 0$ scales for the inertia effect, the parameter $\zeta < 0$ for the R-T instability mechanism, and the parameter

$\eta > 0$ for the viscous dissipation in the streamwise direction. As proposed by Ruyer-Quil and Manneville,[23] an adiabatic elimination of the fields $s_1 = s_2 = 0$ in (1) leads to the following *simplified second-order model*:

$$\partial_t h = -\partial_x q, \tag{2a}$$

$$\delta\partial_t q = \frac{5}{6}h - \frac{5}{2}\frac{q}{h^2} - \delta\frac{17}{7}\frac{q}{h}\partial_x q + \left(\delta\frac{9}{7}\frac{q^2}{h^2} - \frac{5}{6}\zeta h\right)\partial_x h + \frac{5}{6}h\partial_{xxx}h + \eta\left[4\frac{q}{h^2}(\partial_x h)^2 - \frac{9}{2h}\partial_x q\partial_x h - 6\frac{q}{h}\partial_{xx}h + \frac{9}{2}\partial_{xx}q\right]. \tag{2b}$$

It is worth mentioning that the terms in square brackets result from the so-called viscous extensional stress, well known in models for thin viscous sheets[24] for which the extensional term is $4\partial_x(h\partial_x(q/h))$, where 4 is the so-called Trouton ratio. The only differences here stand in the coefficients of each term (apart for the first one), which account for the integration of a parabolic velocity profile, instead of a uniform velocity profile in the case of a free-standing film. If these second-order viscous extensional terms are further neglected, i.e., taking $\eta = 0$, (2) reduces to the *first-order model*, which therefore corresponds to (2a) and the first line of (2b). Finally, neglecting also inertia effects, i.e., for $\delta = 0$, the first-order model reduces, by eliminating q, to a *single long-wave equation* for the film thickness,

$$\partial_t h = -\partial_x\left[\frac{h^3}{3}(1 + \partial_{xxx}h - \zeta\partial_x h)\right]. \tag{3}$$

This equation is identical to the one considered by Duprat *et al.*[25] (except that their β parameter equals $-\zeta$ here), even if another physics is involved since the authors considered a film flowing along a fibre, where the absolute instability mode arises due to the Rayleigh-Plateau instability. Equation (3) has also been recently analysed by Brun *et al.*,[9] who have used another scaling that will be explicated in Section IV B.

The hierarchy of models that have been introduced above is summarised in Figure 2. Most of the results below are obtained with the *full second-order model* since it has been shown by Ruyer-Quil and Manneville[26] to contain all features needed to fit exact linear properties obtained with the Orr–Sommerfeld equations — i.e., the perturbation equations directly obtained from the Navier–Stokes equations. However, the differences between the *full second-order model* and the three other ones will be first examined in Section IV, putting in evidence some important influences of the various effects considered, such as inertia at first- and second-order, and viscous extensional stress.

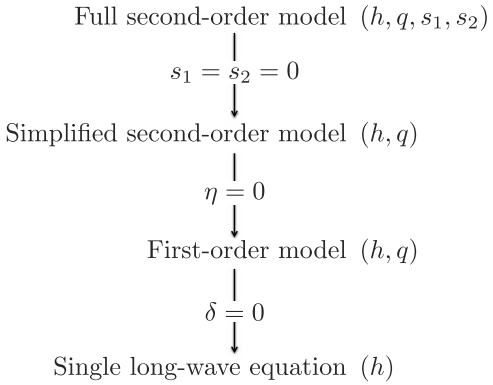

FIG. 2. Hierarchy of averaged models with corresponding dependent variables in parentheses. Each arrow indicates the step to reduce one model to another. The steps are additive.

III. METHODOLOGY

With the aim to identify the linear absolute/convective (A/C) transition, the following normal mode perturbations of the dimensionless flat film solution are considered:

$$h = 1 + a\, e^{i(kx-\omega t)}, \tag{4a}$$

$$q = \frac{1}{3} + b\, e^{i(kx-\omega t)}, \tag{4b}$$

where $k = k_r + ik_i$ and $\omega = \omega_r + i\omega_i$ are complex wavenumber and complex pulsation, respectively, and a and b are complex amplitudes. For the sake of simplicity, the procedure is detailed below with the *simplified second-order model* and then extended to the other models. Inserting (4) into (2), and linearising for $a, b \ll 1$, leads to the following dispersion relation:

$$k^2\left(-\frac{\delta}{7} - \frac{9i\eta\omega}{2} + \frac{5\zeta}{6}\right) + k\left(\frac{17\delta\omega}{21} + \frac{5i}{2}\right) - \delta\omega^2 + 2i\eta k^3 + \frac{5k^4}{6} - \frac{5i\omega}{2} = 0. \tag{5}$$

Following, for instance, Charru,[27] the transition between convective and absolute instabilities is defined by the marginal mode that is neither amplified nor damped, i.e., for $\omega_i = 0$, and located at a fixed position in space. This mode corresponds to a zero group velocity defined as $V = \partial_k\omega$. Considering $\omega = \omega(k)$ in (5), differentiating the equation with respect to k, and prescribing $\partial_k\omega = 0$ lead to

$$2k\left(-\frac{\delta}{7} - \frac{9}{2}i\eta\omega + \frac{5\zeta}{6}\right) + \frac{17}{21}\delta\omega + 6i\eta k^2 + \frac{10k^3}{3} + \frac{5i}{2} = 0. \tag{6}$$

For a given set of parameters (δ, η), the system of complex equations (5) and (6) can be solved for the four real variables k_r, k_i, ω_r, and ζ. Note that the choice of ζ as a variable (instead of δ or η) is arbitrary but convenient. In the case of negligible viscous extensional effects, i.e., for $\eta = 0$, (2) reduces to the *first-order model* and the system of equations to be solved for the A/C transition is merely (5) and (6) in which $\eta = 0$. In the case of $\delta = \eta = 0$ corresponding to the *single long-wave equation* (3), system (5) and (6) reduces to

$$3i\omega = k^4 + k^2\zeta + 3ik, \tag{7a}$$

$$0 = 4k^3 + 2k\zeta + 3i. \tag{7b}$$

The non-trivial real solution of (7), with $k_r > 0$, is

$$\zeta_c^{(0)} = -\frac{3\,3^{2/3}}{\sqrt[3]{2\left(17 + 7\sqrt{7}\right)}} \approx -1.507, \qquad k_r^{(0)} = \sqrt[6]{\frac{153}{256} + \frac{117\sqrt{7}}{512}} \approx 1.03, \tag{8a}$$

$$k_i^{(0)} = -\frac{\sqrt[3]{9 - 3\sqrt{7}}}{2\,2^{2/3}} \approx -0.32, \quad \text{and} \quad \omega_r^{(0)} = \frac{1}{8}\sqrt[3]{3}\sqrt[6]{10\,037 + 3794\sqrt{7}} \approx 0.94. \tag{8b}$$

As anticipated, solution (8) is identical to the one obtained, not only by Brun *et al.* for the R-T instability but also by Duprat *et al.* (2007) for the Rayleigh-Plateau instability in falling films along fibers.

Solution of (5) and (6) that includes inertia and viscous extensional effects can now be tracked by continuation with the software AUTO-07p, using (8) as starting solution. The same procedure can also be applied to *full second-order model* (1) and the system of equations to be solved in this case for the A/C transition is given in Appendix B.

The set of parameters (ζ, δ, η) used so far and referred to as the Shkadov scaling can be converted to a set of more common parameters, namely (*Ct*, *Re*, *We*), corresponding to the inclination number, the Reynolds number, and the Weber number, respectively. The two sets of parameters are related by the following expressions:

$$\zeta = \frac{Ct}{We^{1/3}}, \quad \delta = \frac{3Re}{We^{1/3}}, \quad \text{and} \quad \eta = \frac{1}{We^{2/3}}, \tag{9}$$

whose parameters depend in turn on the physical quantities as follows:

$$Ct = \cot\beta, \quad Re = \frac{g\sin\beta h_N^3}{3\nu^2}, \quad \text{and} \quad We = \frac{\gamma}{\rho g h_N^2 \sin\beta}, \tag{10}$$

where ν is the kinematic viscosity, γ is the surface tension, and ρ is the density of the liquid. The range $0 < \beta < \pi/2$, i.e., $Ct > 0$, corresponds to the situation for which the hydrostatic force stabilises the flow, while the range $\pi/2 < \beta < \pi$, i.e., $Ct < 0$, corresponds to the situation considered in this paper for which the hydrostatic force destabilizes the flow through the R-T mechanism.

IV. RESULTS

A. Shkadov scaling

Results for various values of η are plotted in Figure 3. The solid lines correspond to the transition between absolute instability on the left of the curves and convective instability of the right of the curves, as calculated with the *full second-order model*. The dotted lines are the same transitions calculated with the *simplified second-order model*. The dotted-dashed curve corresponds to the *first-order model*, i.e., the *simplified model* with $\eta = 0$, which slightly differs from the *full second-order model* with $\eta = 0$ as the latter still accounts for second-order inertia effects.

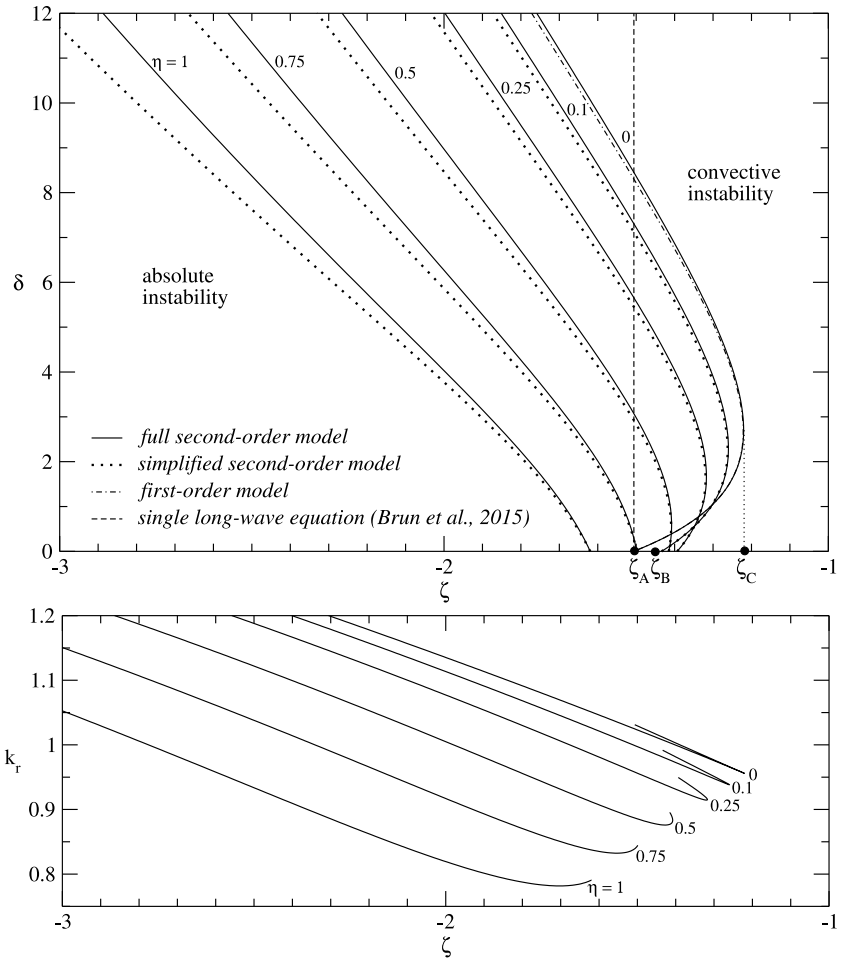

FIG. 3. (Top) Convective/absolute transition for various values of η and for the different models considered in this paper. See details in text for the bullet points. (Bottom) Corresponding values of the wavenumber k_r calculated with the *full second-order model*.

Bullet points in Figure 3 indicate three particular values of ζ as follows:

- $\zeta_A \approx -1.507$ is solution (8b) obtained in the limit of no inertia and no viscous extensional effects;
- $\zeta_B \approx -1.453$ is the limiting value below which the film is absolutely unstable for $\delta = 0$ provided $\eta_B \geq 0.63$;
- $\zeta_C \approx -1.22$ is the limiting value above which the film cannot be absolutely unstable, whatever the values of δ and η.

The differences between the *simplified* and the *full second-order models* are negligible for $\delta < 1$ but increase with δ. As compared to the *first-order model*, viscous extensional stresses play an important role in stabilizing the flow by displacing to lower values of ζ the A/C transition. Similarly, comparing the *first-order model* with the *single long-wave equation* shows a crucial influence of inertia effect, which is non-monotonous for $\eta < \eta_B = 0.63$, i.e., destabilizing for low δ and stabilizing for large δ, whereas it is always stabilizing for $\eta > \eta_B$. In other words, the turning points in some of the curves of Figure 3 indicate the presence of an absolutely unstable window in a range of δ that depends on ζ and η but can only exist for $0 < \eta < \eta_B$ and $\zeta_B < \zeta < \zeta_C$.

The bottom plot in Figure 3 shows the values of the wavenumber k_r corresponding to the A/C transition and calculated only with the *full second-order model*. For a practical point of view, the dimensional wavelength can be calculated as $\lambda_r = 2\pi We^{1/3} h_N / k_r$, which is in general in the millimetre range.

For an inclined plate with the liquid flowing on its underside, both the driving force entraining the liquid to flow along the plate and the hydrostatic destabilising force are induced by gravity and antagonistically depend on the inclination angle β. Additionally, the driving force can be measured by two different ways, depending on the imposed conservation condition, namely, (i) the imposed film thickness and (ii) the imposed flow rate. These conditions are separately examined in Subsections IV B and IV C.

B. Imposed film thickness

The case of an imposed film thickness has recently been studied by Brun *et al.*,[9] who poured a layer of liquid on top of a glass plate and then, after a significantly long resting time, inverted the plate up to a given angle. To be consistent with their study, the same set of independent parameters is adopted in this section, namely, α for the plate inclination taken from the vertical (see Fig. 1) and the initial flat film thickness parameter $h_* = h_N/\ell_c$, where $\ell_c = \sqrt{\gamma/\rho g}$ is the capillary length. Additionally, the Kapitza number is defined as $Ka = (\ell_c/\ell_\nu)^2$, where $\ell_\nu = (\nu^2/g)^{1/3}$ is the viscous/gravity length, hence $Ka = \gamma/(\rho g^{1/3}\nu^{4/3})$. Using the definitions provided in (9) and (10), as well as $\beta = \alpha + \pi/2$, yields the following relations:

$$\zeta = -h_*^{2/3}(\cos\alpha)^{1/3}\tan\alpha, \quad \delta = h_*^{11/3}(\cos\alpha)^{4/3}Ka^{3/2}, \quad \text{and} \quad \eta = h_*^{4/3}(\cos\alpha)^{2/3}. \tag{11}$$

The limit of no inertia and no viscous extensional stress, as considered by Brun *et al.*,[9] is recovered by rearranging the first relation in (11) and using the solution in (8),

$$\tan\alpha_c^{(0)}\sqrt{\sin\alpha_c^{(0)}} = \frac{\left|\zeta_c^{(0)}\right|^{3/2}}{h_*} \approx \frac{1.8495}{h_*}. \tag{12}$$

To account for the effect of inertia, the value of the Kapitza number needs to be specified. Castor oil, as measured by Brun *et al.*,[9] has a capillary length of $\ell_c = 1.91$ mm and a viscous length of $\ell_\nu = 4.7$ mm, with the kinematic viscosity of 0.001 m^2/s at 20 °C. This yields a Kapitza number of $Ka = 0.17$, which is in the lower range of common values for this number.

Figure 4 shows the critical angle for the A/C instability transition versus the dimensionless thickness h_* for various values of the Kapitza number. Obviously, and for any fixed value of h_*, the film is absolutely unstable as the plate inclination tends to the horizontal, i.e., $\alpha \to 90°$, while there is always a critical angle α_c below which the system becomes convectively unstable. This critical angle does not vary monotonically with h_*, which constitutes one of the main findings of this

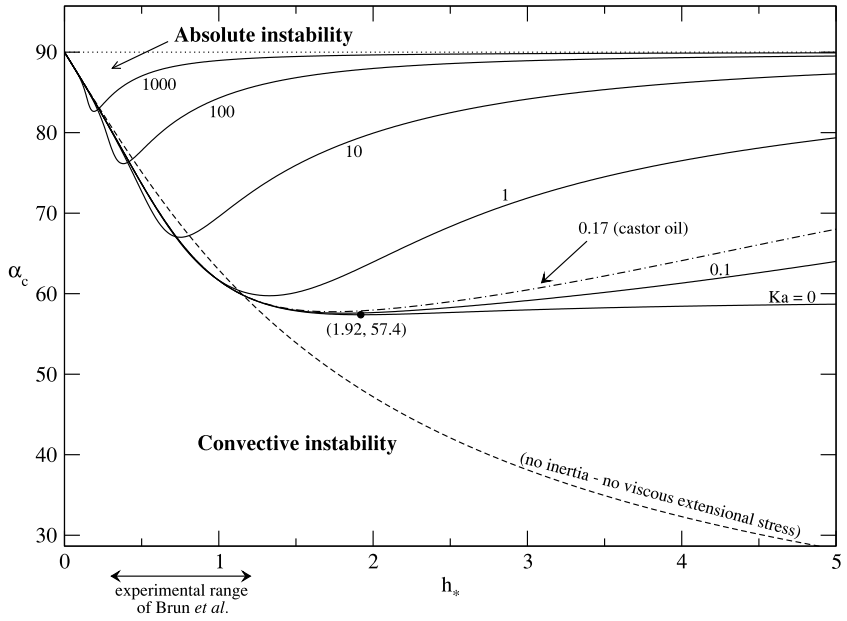

FIG. 4. Critical inclination angle α_c for convective/absolute transition for various values of Ka as obtained with the *full-second-order model* (solid lines). The black dot indicates the position of the minimum in the case of $Ka = 0$. The curve corresponding to castor oil is in dotted-dashed line and the one corresponding to (12) obtained with the *single long-wave equation*, i.e., $\alpha_c^{(0)}$, is in dashed line.

work. For small values of h_*, i.e., on the left of the curve minimum, α_c decreases with increasing h_* showing a "destabilizing" effect of the flow, in the sense that the region of absolute instability is enlarged. For larger values of h_*, i.e., at the right of the curve minimum, α_c increases with h_*, which in turn shows a "stabilizing" effect of the flow, in the sense that the region of absolute instability is reduced, even though this is less pronounced for the lowest values of the Kapitza number.

The antagonist role of the flow can be understood, for instance, by fixing the inclination angle and increasing h_* from zero. Small thickness triggers small amplitude waves, which can prevent the absolute instability to occur, whereas larger thickness triggers larger amplitude waves, which can reinforce the R-T instability mechanism and bring the system into the absolute instability region. As the thickness is still increased, the flow dominates the system again and brings it back into the convective instability region.

Additionally, the critical angle strongly depends on the Kapitza number. Increasing the Kapitza number decreases the region of absolute instability and sharpens the curves around their minima. These minima are also shifted to lower values of the film thickness with increasing Kapitza number, especially evident for $Ka = 1000$, which is in the order of magnitude of low viscous fluids and/or high surface tension, like water. Remarkably, in the limit of $Ka \to 0$, this minimum critical angle does not go below an angle of $\alpha = 57.3875° \approx 57.4°$, which is indicated by the black dot in Fig. 4. This result represents a fundamental difference with the results of Brun *et al.*[9] in the limit of no-inertia, which does not show any minimum (see dashed line in Fig. 4). In our scaling, and as shown in (11), $Ka = 0$ indeed corresponds to no inertia effects since it cancels out the reduced Reynolds number δ. Yet viscous extensional stress has already a strong influence in this no-inertia limit, as it prevents alone the flow to be absolutely unstable below the curve minimum (black dot).

The curve corresponding to castor oil is represented in dotted-dashed line in Fig. 4, showing that the film cannot be absolutely unstable for an angle from the vertical below approximately 58°, which agrees with the experimental observations of Brun *et al.*[9] The range of thickness covered by the experiment of Brun *et al.* is $0.3 \le h_* \le 1.2$, in which (12) remains a fair approximation.

However, and as already mentioned, for $h_* > 1.2$ inertia and viscous extensional effects become significant, which makes approximation (12) unusable in this range.

C. Imposed flow rate

For a film fed at a constant flow rate q_N, the relevant parameter is the Reynolds number, defined in (10) and equivalently equal to $Re = q_N/\nu$. Following the same procedure as in Sec. IV B, the relations between the parameters become

$$\zeta = -\frac{(3Re)^{2/9}\sin\alpha}{Ka^{1/3}(\cos\alpha)^{8/9}}, \quad \delta = \frac{(3Re)^{11/9}(\cos\alpha)^{1/9}}{Ka^{1/3}}, \quad \text{and} \quad \eta = \frac{(3Re)^{4/9}(\cos\alpha)^{2/9}}{Ka^{2/3}}. \tag{13}$$

The limit of no inertia and no viscous extensional stress corresponds to

$$(\tan\alpha_c^{(0)})^4\sqrt{\sin\alpha_c^{(0)}} = \left|\zeta_c^{(0)}\right|^{9/2}\frac{Ka^{3/2}}{3Re} \approx 2.1086\frac{Ka^{3/2}}{Re}. \tag{14}$$

Figure 5 shows the critical angle for the A/C instability transition versus the Reynolds number Re for various values of Ka. The branches on the left of the minima for each curve (see black dots) can fairly be approximated by (14) (not shown) but again the curve minimum and the right branches are not captured by this approximation. At high Reynolds numbers, the convective transport dominates the growth of the R-T instability for which the film flow is convectively unstable. In the high Reynolds number regime, the Kapitza number (surface tension) has less significant influence, for which the curves for the various values of Ka more or less converge. Decreasing the flow rate in this range results also in a reduction of the propagation speed, owing to the strong correlation between wave velocity and surface velocity. As a consequence, the convective transport of the R-T instability is low. In order to remain in the regime of convective instability, the destabilizing component of gravity $g\cos\alpha$ needs to be reduced, decreasing the growth of R-T instability. Thus, the value of the critical angle reduces with the decrease of the Reynolds number down to the minimum value

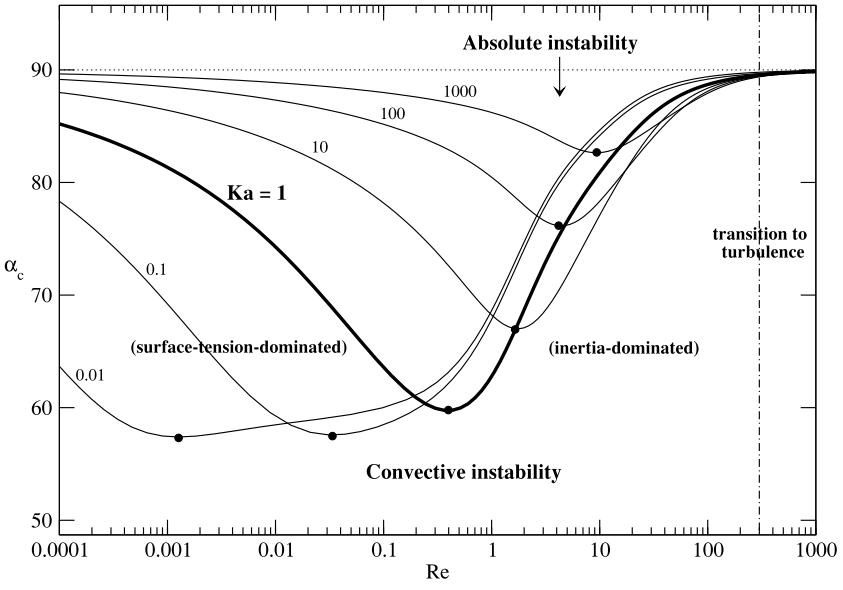

FIG. 5. Convective/absolute transition for various values of Ka as obtained with the *full-second-order model*. The thick solid line for $Ka = 1$ is to exemplify that the convective instability region below the curve is dominated by surface tension on the left and by inertia on the right, while the region above the curve corresponds to the absolute instability. These observations apply to all other curves. The black dots indicate the position of $\alpha_c^{\min}$ for each Ka, the locus of which is continued in Fig. 6(a). The vertical dotted-dashed line indicates the transition for turbulence, which lies outside the range of validity of the present theory.

of the critical inclination angle. Below this value, surface tension is the main mechanism of flow stabilization as seen by the significant influence of Kapitza number.

Based on these observations, and as exemplified in the case of $Ka = 1$ in Fig. 5 (thick solid line), one can state that the region of convective instability on the left of the minimum value of the critical angle is dominated by surface tension while the region of convective instability which lies on the right of this minimum is dominated by inertia. The region of absolute instability in between is dominated by the negative hydrostatic forces responsible for the R-T instability.

We have drawn in Fig. 5 a vertical dotted-dashed line that indicates the transition between laminar and turbulent falling films,[28] which is approximately considered to be at $Re \approx 300$. Even though we have plotted the A/C transition curve up to $Re = 1000$ in order to show that all curves asymptotically tend to $\alpha = 90°$, these curves obviously lay outside the domain of validity of the low-dimensional models that have been used in this work. This said, and as already mentioned, comparisons of linear stability curves between the *full second-order model* and the Orr-Sommerfeld equation show excellent agreement for $Re = O(100)$,[3,26] which justifies our computations up to Reynolds numbers of the same order of magnitude.

D. Minimum critical angle

In Subsections IV B and IV C, Figs. 4 and 5 showed that for each value of the Kapitza number a minimum critical angle $\alpha_c^{\min}$ is given below which the falling film is always convectively unstable, independently of the conservation condition (constant flow rate or constant film thickness). Figure 6(a) shows the locus of this minimum critical angle in the entire range of Kapitza numbers. Now, above the minimum critical angle, the film can either be convectively or absolutely unstable,

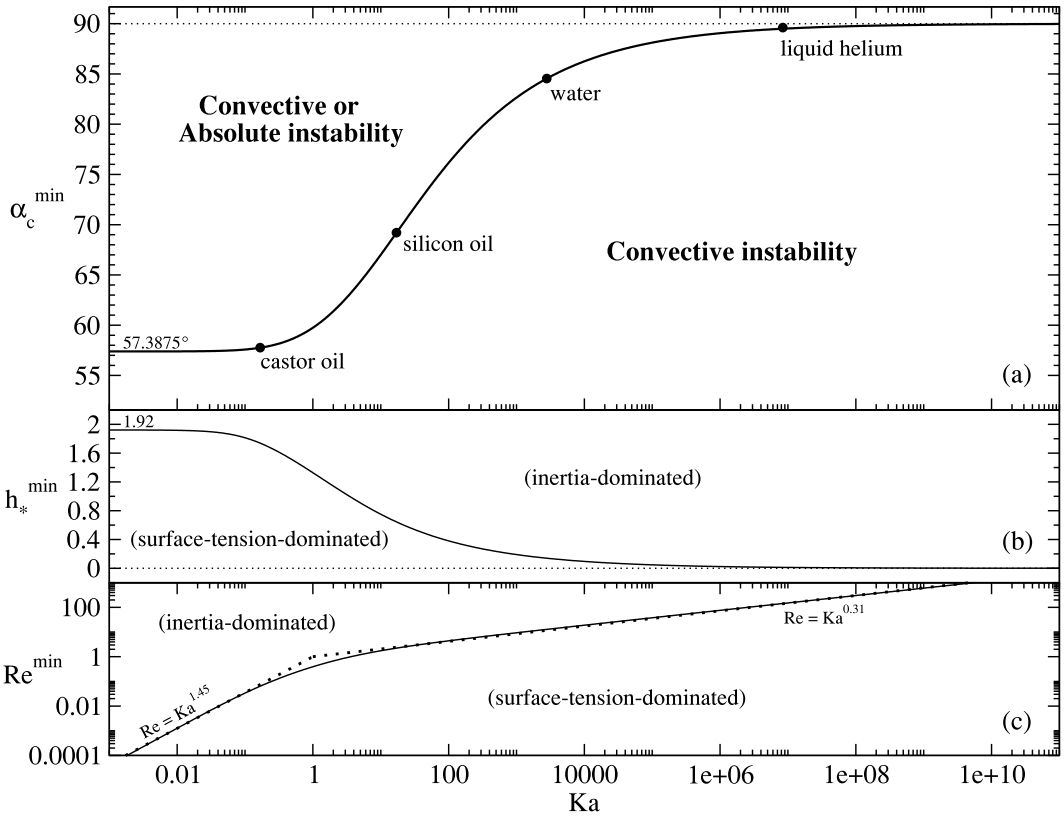

FIG. 6. Minimum critical angle between absolute and convective instabilities, in function of the Kapitza number (a), along which the corresponding values of the dimensionless film thickness (b) or alternatively the Reynolds number (c). In (c), thick dotted lines are fitted power trends together with their expressions.

depending on the flow parameters, i.e., h_* or Re. What we have learned from Fig. 5 is that for $\alpha_c > \alpha_c^{\min}$ there is a region of absolute instability that separates a region of convective instability dominated by surface tension and a region of convective instability dominated by inertia. Plotting in Figs. 6(b) and 6(c) the positions $h_*^{\min}$ and $Re^{\min}$, respectively, corresponding to the minimum critical angle allows to discriminate in the parameter space between these two regions.

In Fig. 6(a), the minimum critical angles are indicated by black dots for castor oil ($Ka = 0.17$), silicon oil 20 times more viscous than water at 25 °C ($Ka = 17.8$), water at 25 °C ($Ka = 3923$), and liquid helium at 5 K ($Ka = 8.6 \times 10^6$). As already pointed out, the most salient feature is that there is an angle $\alpha_c^{\min}|_{Ka\to 0} = 57.3875°$ obtained in the limit of $Ka \to 0$ corresponding to an infinitely viscous fluid below which none of the liquid film systems can be absolutely unstable. For real liquids of finite viscosity, such as for 20 cP silicon oil, this minimum critical angle is 69°, for water it is 84.5°, and for liquid helium it is 89°.

V. DISCUSSION

Our approach for computing the A/C instability transition curves has implicitly consisted in tracking by continuation of the dominant saddle point in the complex plane (k_r, k_i), which is the one having the highest growth rate,[29] namely, the one satisfying the so-called "collision criterion" established by Briggs.[30] The starting saddle point for the tracking method was the one obtained analytically in the limit of no inertia ($\delta \to 0$) and no viscous extensional stress ($\eta \to 0$) as given by (8). The symmetry properties of the dispersion relation for *single long-wave equation* (7a) ensure the obtained saddle-point to be the only viable candidate. This is no longer true for the dispersion relations of the *simplified* and the *full second-order models*, i.e., (5) and (B1a), respectively.

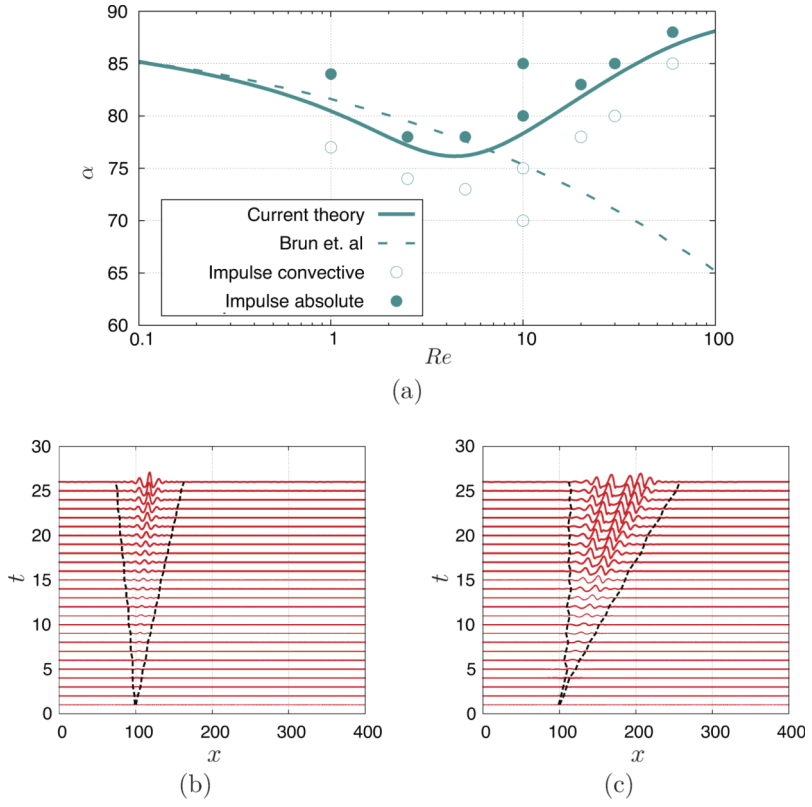

FIG. 7. Verification of the current theory using direct numerical simulations of the impulse response computed with Gerris for $Ka = 100$: (a) comparison to the transition curve obtained with the *full second-order model*, (b) spatio-temporal diagram showing an absolute instability behaviour for $\alpha = 85°$, $Re = 10$, and (c) a convective instability behaviour for $\alpha = 70°$, $Re = 10$. The dashed lines in (b) and (c) show the edges of the wavepacket (see text for details).

There are other saddle points and we have therefore no guarantee that the one found by continuation is effectively the dominant one in the entire parameter domain explored in this study. Some examples in the literature indeed show that misleading or subdominant saddle points had to be disregarded.[31–34]

Instead of looking at the structure of the spatial branches throughout the entire continuation procedure, which represents a tedious task, we propose here another method to verify that the A/C transition identified in this paper corresponds to the dominant saddle point. For that purpose, we compute the system impulse response using direct numerical simulation. More specifically, we employ Gerris which is an open-source software that uses the VOF method and adaptive refinement of quadtree meshes.[35] The initial state of our computations is a uniform film in a long periodic domain with a small amplitude sharp Gaussian pulse situated at one forth of the domain length. We adjust the pulse amplitude for each simulation in order to visualize the evolution of the wave packet. Even though we cannot distinguish with this approach between the linear and the nonlinear impulse responses of the flow, these properties coincide with each other most of the time,[36] as it is assumed to be the case here.

Figure 7(a) compares for a fixed Kapitza number the transition curve obtained with the *full second-order model* to the impulse response behaviour of the flow computed with Gerris. The agreement is convincing especially in the sense that it captures well the minimum of the A/C transition curve, which is the main difference between our theory and the one by Brun *et al.*[9] Very close to the curve, it becomes difficult to conclude on the absolute/convective nature of the response because the edges of the wavepacket oscillate (see Figures 7(b) and 7(c)). These oscillations are simply due to the way the edges (dashed lines) are constructed, based on the following threshold criterion: $|h-1| = A$, with $5\times10^{-3} < A < 5\times10^{-2}$ adjusted for the different inclination angles and Reynolds numbers. Notice that the analysis has been restricted to the range $1 < Re < 60$. For $Re < 1$, the instability growth rate is very low which means long computational time. On the contrary for $Re > 60$, the instability growth rate is very large and numerical noise is rapidly amplified. Note that for $Re < 1$, the transition curve obtained with the *full second-order model* is very close to the one obtained with the *single long-wave equation*,[9] which is a proof by itself that the dominant saddle-point is well captured in this range.

VI. CONCLUSIONS

This study examined the critical inclination angle for the transition from absolute to convective instability of falling liquid films flowing on the underside of a plate. The results are based on the weighted integral boundary layer models which has been proven by many studies to give reliable results in the laminar regime of falling liquid films. The transition between the absolute and convective instabilities is obtained by tracking the marginal mode that is neither amplified nor damped and located at a fixed position in space. Tracking the transition for the case of a constant film thickness, a strong dependency on Kapitza number has been obtained. Furthermore, a significant "stabilizing" effect of viscous extensional stress has been identified, especially for a dimensionless film thickness larger than unity. If the flow rate is imposed as a conservation condition, the stabilizing mechanism of surface tension (dependent on Kapitza number) becomes apparent for low values of the Reynolds number. Contrarily, for high Reynolds number, the convective transport (hence inertia effects) dominates such that surface tension is of minor importance.

The A/C transition has been found by continuation of the most dominant saddle point from the limit of no inertia and no viscous extensional stress, i.e., by continuously increasing δ and η from zero. The validity of this approach has been checked by computing the system impulse response using direct numerical simulations. The agreement for the A/C transition is convincing over the entire range of relevant Reynolds numbers.

Finally, a minimum critical angle depending on the Kapitza number has been identified which is independent from the conservation condition (imposed flow rate or imposed film thickness). Since the Kapitza number depends on the fluid properties and on gravity only, each fluid has its own minimum critical angle on the earth. This minimum critical angle decreases with decreasing Kapitza number, such that a higher gravitational force driving the flow is necessary for low Kapitza

number fluids. Contrarily, high Kapitza number fluids such as Water (Ka = 3923 at 20 °C), where surface tension stabilizes the flow, allow for high inclination angles of approximately 85° (from the vertical) before the instability changes from convective to absolute. This might have a practical interest in architectural applications as a condensed film forming on a ceiling would never be absolutely unstable if the ceiling is inclined by an angle of about 5° (from the horizontal), whatever the film thickness. This is the reason why the ceiling of hammams is always curved. The determination of the critical angle in falling films evaporators that often have some section with negative hydrostatic forces could help in enhancing the design of these devices and avoid clogging.

ACKNOWLEDGMENTS

We are deeply grateful to François Gallaire for fruitful discussions. We acknowledge the financial support of EU-FP7 ITN Multiflow as well as the BELSPO agency under the Grant No. IAP-7/38 MicroMAST. B.S. also thanks the F.R.S.-FNRS for financial support. This research has been performed under the umbrella of the COST Action No. MP1106.

APPENDIX A: FULL SECOND-ORDER MODEL

Following the weighted residuals methodology detailed, e.g., in Kalliadasis *et al.*,[3] and using the two-dimensional system of reference as defined in Fig. 1(a), the streamwise velocity field is projected onto the following polynomials:

$$F_0 = \bar{y} - \frac{1}{2}\bar{y}^2, \tag{A1a}$$

$$F_1 = \bar{y} - \frac{17}{6}\bar{y}^2 + \frac{7}{3}\bar{y}^3 - \frac{7}{12}\bar{y}^4, \tag{A1b}$$

$$F_2 = \bar{y} - \frac{13}{2}\bar{y}^2 + \frac{57}{4}\bar{y}^3 - \frac{111}{8}\bar{y}^4 + \frac{99}{16}\bar{y}^5 - \frac{33}{32}\bar{y}^6. \tag{A1c}$$

The streamwise velocity distribution thus reads

$$u = \frac{3}{h}(q - s_1 - s_2)\, g_0(\bar{y}) + 45\frac{s_1}{h} g_1(\bar{y}) + 210\frac{s_2}{h} g_2(\bar{y}), \tag{A2}$$

where $\bar{y} = y/h$ and the flow rate $q(x,t) = \int_0^{h(x)} u(x,y,t)\,\mathrm{d}y$ appears with two corrections, namely, s_1 and s_2.

Applying the Galerkin method, which consists of integrating the classical boundary-layer equations across the film, substituting projections (A2) into the integrated equations, taking test functions (A1) as weight functions, and using the no-slip boundary condition at the wall and the stress-free condition at the interface yield the *full second-order model* given in (1). Note that (1b) is different than the equation for q given in Ruyer-Quil and Manneville[23] because the terms $\delta\partial_t s_1$ and $\delta\partial_t s_2$ have not been substituted here by (1c) and (1d), respectively, in order to enable the straightforward adiabatic elimination of s_1 and s_2 leading to the *simplified second-order model*.

APPENDIX B: SYSTEM OF EQUATIONS FOR THE A/C TRANSITION WITH THE FULL SECOND-ORDER MODEL

$$\begin{aligned}
0 = {} & 3i\omega + \frac{18\delta\omega^2}{13} - \frac{10}{143}i\delta^2\omega^3 - \frac{4\delta^3\omega^4}{6435} + k\left(\frac{4\delta^3\omega^3}{5005} + \frac{98i\delta^2\omega^2}{1287} - \frac{174\delta\omega}{143} - 3i\right) \\
& + k^2\left(-\frac{2027i\delta^2\eta\omega^3}{720\,720} + \omega\left(-\frac{2936i\delta^2}{117\,117} + \frac{4i\delta\zeta}{65} + \frac{27i\eta}{5}\right)\right. \\
& \qquad \left. + \omega^2\left(-\frac{68\delta^3}{195\,195} + \frac{3\delta^2\zeta}{5005} + \frac{1077\delta\eta}{3640}\right) + \frac{166\delta}{715} - \zeta\right) \\
& + k^3\left(\frac{3439i\delta^2\eta\omega^2}{1\,310\,400} + \frac{152i\delta^2}{65\,065} + \omega\left(\frac{368\delta^3}{6\,441\,435} - \frac{16\delta^2\zeta}{45\,045} - \frac{2441\delta\eta}{12\,012}\right) - \frac{304i\delta\zeta}{15\,015} - \frac{12i\eta}{5}\right)
\end{aligned}$$

$$+k^4\left(-\frac{16\delta^3}{6\,441\,435}+\omega\left(\frac{4i\delta}{65}-\frac{4591i\delta^2\eta}{5\,855\,850}\right)+\frac{3\delta^2\omega^2}{5005}+\frac{148\delta^2\zeta}{2\,927\,925}+\frac{10\,331\delta\eta}{320\,320}-1\right)$$
$$+k^5\left(\frac{197i\delta^2\eta}{2\,602\,600}-\frac{16\delta^2\omega}{45\,045}-\frac{304i\delta}{15\,015}\right)+k^6\frac{148\delta^2}{2\,927\,925}, \tag{B1a}$$

$$0=-3i-\frac{174\delta\omega}{143}+\frac{98i\delta^2\omega^2}{1287}+\frac{4\delta^3\omega^3}{5005}+k\left(-\frac{2027i\delta^2\eta\omega^3}{360\,360}+2\omega\left(-\frac{2936i\delta^2}{117\,117}+\frac{4i\delta\zeta}{65}+\frac{27i\eta}{5}\right)\right.$$
$$\left.+2\omega^2\left(-\frac{68\delta^3}{195\,195}+\frac{3\delta^2\zeta}{5005}+\frac{1077\delta\eta}{3640}\right)+\frac{332\delta}{715}-2\zeta\right)$$
$$+k^2\left(\frac{3439i\delta^2\eta\omega^2}{436\,800}+\frac{456i\delta^2}{65\,065}+3\omega\left(\frac{368\delta^3}{6\,441\,435}-\frac{16\delta^2\zeta}{45\,045}-\frac{2441\delta\eta}{12\,012}\right)-\frac{304i\delta\zeta}{5005}-\frac{36i\eta}{5}\right)$$
$$+k^3\left(-\frac{64\delta^3}{6\,441\,435}+4\omega\left(\frac{4i\delta}{65}-\frac{4591i\delta^2\eta}{5\,855\,850}\right)+\frac{12\delta^2\omega^2}{5005}+\frac{592\delta^2\zeta}{2\,927\,925}+\frac{10\,331\delta\eta}{80\,080}-4\right)$$
$$+k^4\left(\frac{197i\delta^2\eta}{520\,520}-\frac{16\delta^2\omega}{9009}-\frac{304i\delta}{3003}\right)+k^5\frac{296\delta^2}{975\,975}. \tag{B1b}$$

[1] H.-C. Chang and E. Demekhin, in *Complex Wave Dynamics on Thin Films*, edited by D. Möbius and R. Miller (Elsevier, Amsterdam, 2002).
[2] S. V. Alekseenko, V. E. Nakoryakov, and B. G. Pokusaev, in *Wave Flow of Liquid Films*, edited by T. Fukano (Begell House, New York, 1994).
[3] S. Kalliadasis, C. Ruyer-Quil, B. Scheid, and M. Velarde, *Falling Liquid Films* (Spinger-Verlag, 2012), p. 440.
[4] G. F. Dietze, A. Leefken, and R. Kneer, "Investigation of the backflow phenomenon in falling liquid films," J. Fluid Mech. **595**, 435–459 (2008).
[5] W. Rohlfs and B. Scheid, "Phase diagram for the onset of circulating waves and flow reversal in inclined falling films," J. Fluid Mech. **763**, 322–351 (2015).
[6] J. Liu, J. D. Paul, and J. P. Gollub, "Measurements of primary instability of film flows," J. Fluid Mech. **250**, 69–101 (1993).
[7] Lord Rayleigh, "Investigation of the character of the equilibrium of an incompressible heavy fluid of variable density," Proc. London Math. Soc. **s1-14**, 170–177 (1883).
[8] S. Chandrasekhar, *Hydrodynamics and Hydromagnetic Stability* (Oxford University Press, 1961).
[9] P.-T. Brun, A. Damiano, P. Rieu, G. Balestra, and F. Gallaire, "Rayleigh-Taylor instability under an inclined plane," Phys. Fluids **27**, 084107 (2015).
[10] A. L. Frenkel and D. Halpern, "On saturation of Rayleigh-Taylor instability," in *IUTAM Symposium on Nonlinear Waves in Multi-Phase Flow*, Fluid Mechanics and Its Applications Vol. 57, edited by H.-C. Chang (Springer, Netherlands, 2000), pp. 69–79.
[11] M. Fermigier, L. Limat, J. E. Wesfreid, P. Boudinet, and C. Quilliet, "Two-dimensional patterns in Rayleigh-Taylor instability of a thin layer," J. Fluid Mech. **236**, 349–383 (1992).
[12] G. H. Wolf, "Dynamic stabilization of interchange instability of a liquid-gas interface," Phys. Rev. Lett. **24**, 444–446 (1970).
[13] E. Talib and A. Juel, "Instability of a viscous interface under horizontal oscillation," Phys. Fluids **19**, 092102 (2007).
[14] N. A. Bezdenezhnykh, V. A. Briskman, A. A. Cherepanov, and M. T. Sharov, "Control of the stability of liquid surfaces by means of variable fields," Fluid Mech. - Sov. Res. **15**, 11–32 (1986).
[15] B. K. Kopbosynov and V. V. Pukhnachev, "Thermocapillary flow in thin liquid films," Fluid Mech. - Sov. Res. **95**, 15 (1986).
[16] R. J. Deissler and A. Oron, "Stable localized patterns in thin liquid films," Phys. Rev. Lett. **68**, 2948–2951 (1992).
[17] A. Alexeev and A. Oron, "Suppression of the Rayleigh-Taylor instability of thin liquid films by the Marangoni effect," Phys. Fluids **19**, 082101 (2007).
[18] P. Trinh, H. Kim, N. Hammoud, P. Howell, S. Chapman, and H. Stone, "Curvature suppresses the Rayleigh-Taylor instability," Phys. Fluids **26**, 051704 (2014).
[19] A. J. Babchin, A. L. Frenkel, B. G. Levich, and G. I. Sivashinsky, "Nonlinear saturation of Rayleigh-Taylor instability in thin films," Phys. Fluids **26**, 3159–3161 (1983).
[20] T.-S. Lin, L. Kondic, and A. Filippov, "Thin films flowing down inverted substrates: Three-dimensional flow," Phys. Fluids **24**, 022105 (2012).
[21] S. J. Leib and M. E. Goldstein, "Convective and absolute instability of a viscous liquid jet," Phys. Fluids **29**, 952–954 (1986).
[22] J. Eggers and E. Villermaux, "Physics of liquid jets," Rep. Prog. Phys. **71**, 036601 (2008).
[23] C. Ruyer-Quil and P. Manneville, "Improved modeling of flows down inclined planes," Eur. Phys. J. B **15**, 357–369 (2000).
[24] P. Howell, "Models for thin viscous sheets," Eur. J. Appl. Math. **7**, 321–343 (1996).
[25] C. Duprat, C. Ruyer-Quil, S. Kalliadasis, and F. Giorgiutti-Dauphiné, "Absolute and convective instabilities of a viscous film flowing down a vertical fiber," Phys. Rev. Lett. **98**, 244502 (2007).
[26] C. Ruyer-Quil and P. Manneville, "Further accuracy and convergence results on the modeling of flows down inclined planes by weighted-residual approximations," Phys. Fluids (1994-present) **14**, 170–183 (2002).
[27] F. Charru, *Hydrodynamics Instability* (Cambridge University Press, 2011).
[28] H.-C. Chang, "Wave evolution on a falling film," Annu. Rev. Fluid Mech. **26**, 103–136 (1994).
[29] P. Huerre and P. A. Monkewitz, "Local and global instabilities in spatially developing flows," Annu. Rev. Fluid Mech. **22**, 473–537 (1990).

[30] R. Briggs, *Electron-Stream Interaction with Plasmas* (MIT Press, Cambridge, 1964).
[31] J. J. Healey, "On the relation between the viscous and inviscid absolute instabilities of the rotating-disk boundary layer," J. Fluid Mech. **511**, 179–199 (2004).
[32] J. Healey, "Destabilizing effects of confinement on homogeneous mixing layers," J. Fluid Mech. **623**, 241 (2009).
[33] M. Juniper, "The effect of confinement on the stability of two-dimensional shear flows," J. Fluid Mech. **565**, 171 (2006).
[34] C. Leclercq, B. Pier, and J. Scott, "Absolute instabilities in eccentric Taylor-Couette-Poiseuille flow," J. Fluid Mech. **741**, 543–566 (2014).
[35] S. Popinet, "An accurate adaptive solver for surface-tension-driven interfacial flows," J. Comput. Phys. **228**, 5838–5866 (2009).
[36] I. Delbende and J. M. Chomaz, "Nonlinear convective/absolute instabilities in parallel two-dimensional wakes," Phys. Fluids **10**, 2724 (1998).